applied sciences

MDPI

Article

Experimental Study on Prefabricated Steel Fiber-Reinforced Concrete Casing Arch Method for Strengthening Cracked Lining in Confined Spaces

Yu Zhou [1,2], Zhi Lin [3,*], Lili Liu [3] and Jianghao Zhou [3]

[1] Guangdong Hualu Transport Technology Co., Ltd., Guangzhou 510100, China; 622220970126@mails.cqjtu.edu.cn
[2] Guangdong Provincial Key Laboratory of Tunnel Safety and Emergency Support Technology & Equipment, Guangzhou 510100, China
[3] State Key Laboratory of Mountain Bridge and Tunnel Engineering, College of Civil Engineering, Chongqing Jiaotong University, Chongqing 400074, China; 622220970164@cqjtu.email.com (L.L.); 622230980083@cqjtu.email.com (J.Z.)
* Correspondence: zhilin@cqjtu.edu.cn

Abstract: Increasingly, research indicates that steel fibers can significantly enhance the engineering properties of mortar and concrete; however, few studies have examined their impact on the reinforcement of in-service tunnel linings within sleeve arch structures. In this study, a series of 1:2 scale experiments were conducted using a specialized loading device to compare the reinforcement performance of steel fiber-reinforced concrete sleeve arches and traditional reinforced concrete sleeve arches on prefabricated cracks with depths of 1/3 and 2/3 of the lining thickness. The experimental results were validated using numerical simulations. The results indicate that under the same load, when reinforcing components with 2/3 prefabricated cracks, the maximum compressive strains for steel fiber-reinforced and reinforced concrete sleeve arches were −852 με and −985 με, respectively, and the maximum deflections were 3.57 mm and 5.48 mm. Composite sleeve arches of both materials provide a certain degree of reinforcement to linings with varying damage. The reinforcement performance of steel fiber-reinforced concrete sleeve arches is superior to that of traditional reinforced concrete sleeve arches, with particularly significant reinforcement for linings with 2/3 prefabricated cracks. Numerical simulations have shown that the stress in reinforced concrete at the concentrated stress regions is 16.15%, 6.01%, 12.68%, 36.62%, and 4.82% higher than that in steel fiber-reinforced concrete, respectively, thereby validating the reliability of the experimental results. Therefore, this study recommends the application of steel fiber materials in sleeve arches to achieve superior maintenance and reinforcement, addressing cracking issues in in-service tunnel linings and thereby improving the safety and durability of these structures.

Keywords: highway tunnel; lining reinforcement; prefabricated thin arch; steel fiber concrete; mechanical property

Citation: Zhou, Y.; Lin, Z.; Liu, L.; Zhou, J. Experimental Study on Prefabricated Steel Fiber-Reinforced Concrete Casing Arch Method for Strengthening Cracked Lining in Confined Spaces. *Appl. Sci.* **2024**, *14*, 5941. https://doi.org/10.3390/app14135941

Academic Editor: Syed Minhaj Saleem Kazmi

Received: 3 June 2024
Revised: 26 June 2024
Accepted: 26 June 2024
Published: 8 July 2024

1. Introduction

Tunneling has experienced significant growth worldwide due to advancements in transportation infrastructure and underground construction technologies, becoming a crucial component of major transportation modes, namely highways and railways [1]. As tunnel construction in China rapidly progresses, the scale of such projects continues to expand, with increasing public demands for higher construction standards. Beyond meeting travel demands through additional tunnels, there is a critical need to focus on ensuring operational safety and facilitating subsequent maintenance. Consequently, enhancing the management and maintenance of these tunnel projects is now a pivotal concern [2].

Over time, tunnel linings may deform, crack, or peel off [3,4], compromising both the stability and safety of the tunnel and complicating traffic operations within it. For instance,

the Dugong Ling Tunnel [5,6] in Shanxi Province, China, developed numerous cracks during operation, with fractures ranging up to 5 cm, 10 cm, and even wider. These cracks affect not only the tunnel's safety but also its structural stability. Since its inception, the Shiziya Tunnel on National Highway 209 has experienced issues like pavement cracking and lining collapse due to construction quality, posing significant security risks to tunnel traffic. The Wenchuan earthquake induced substantial deformations and severe lining cracks in the Guxi Tunnel, impacting its overall structural integrity. Furthermore, the lining cracks have led to deformations in the tunnel's rock mass, seriously jeopardizing its structural integrity and safety [7,8].

To address the limitations of ordinary reinforced concrete's poor crack resistance and weak ductility [9], numerous experts and scholars have shifted their focus to steel fiber research. Introducing steel fibers into concrete significantly enhances a variety of engineering properties, including impact strength, toughness, tensile strength, bending strength, and fatigue strength, while also improving spalling resistance [10–13]. Furthermore, incorporating steel fibers renders concrete more homogeneous, transitioning it from a brittle to a more ductile material. When cracks form in concrete, randomly oriented steel fibers help prevent the formation of micro-cracks, limit crack propagation, and enhance both the strength and ductility of the material.

In light of the aforementioned examples, Tian et al. [13,14] employed a thin composite arch structure reinforcement approach using sprayed steel fiber-reinforced concrete light rail to integrate the reinforced body with the original lining, forming a unified structure with enhanced integrity. Su et al. [15] employed finite element analysis to evaluate the stress distribution within the secondary lining and the concrete arch, both prior to and following the application of shotcrete arch reinforcement. Wang et al. [16] investigated the impact of steel fiber-reinforced concrete linings on controlling surrounding rock displacement, reducing lining pressure, and enhancing both the overall and local stability of the supporting structure. Hu et al. [17] conducted research on the use and efficacy of steel fiber shotcrete in single-layer lining structures for tunnel construction. Cui et al. [18] explored the mechanical properties of single-layer steel fiber shotcrete linings and their application in tunnel engineering. He et al. [19] investigated the mix design and construction processes of steel fiber shotcrete. It is evident that many applications of steel fibers in tunnel research focus on their integration during the construction phase within the concrete lining; however, research on the reinforcement of damaged concrete linings using steel fiber-reinforced concrete arches is scarce.

Steel fiber-reinforced concrete differs from ordinary concrete in that it possesses high strength, excellent crack resistance, and substantial resistance to external impacts [20,21]. Numerous experiments have demonstrated that the addition of steel fibers significantly enhances the toughness of concrete under compression. When cracks form in concrete, the stirrup effect of steel fibers within a compressed concrete column becomes evident, causing the structure to crack without leading to fractures or significant damage. This effect helps maintain the integrity of the original structure [22,23]. The application of steel fiber-reinforced concrete technology in tunnel construction enhances the safety and stability of tunnel structures. Research in this domain would strengthen the original lining's structural properties, significantly increase its load-bearing capacity, effectively prevent the propagation of secondary cracks, and enhance overall tunnel safety.

This study aims to bridge this knowledge gap. Initially, a 1:2 scale test was used to compare and analyze the reinforcement performance of steel fiber concrete and traditional reinforced concrete. Subsequently, the reinforcement effects of steel fiber-reinforced concrete arches on 1/3 and 2/3 prefabricated crack linings were analyzed using numerical methods. Finally, a method involving steel fiber-reinforced concrete arches is proposed to enhance the safety of damaged linings.

2. Experimental Design and Loading Scheme

2.1. Experimental Purposes

In the structural design of steel-concrete arches, the crucial aspect is comparing the reinforcement performance between steel fiber-reinforced concrete and traditional reinforced concrete. Consequently, this paper investigates the reinforcement mechanical properties across various arch materials and thicknesses at the cracks, comparing their load capacity, structural deformation, bending stiffness under load, and failure modes. Thus, the potential value of using steel fiber-reinforced concrete for arch reinforcement in tunnels is demonstrated.

2.2. Specimen

The original lining specimens measured 1200 mm in length, 200 mm in thickness, and 250 mm in width, constructed from plain concrete C25. The dimensions of the precast cracks matched those of the original lining. These cracks were simulated by inserting metal plates, 2 mm thick and 25 cm wide, at heights of 66.67 mm and 133.33 mm, into the unset concrete. The arch specimens featured dimensions of 1200 mm in length, 75 mm in thickness, and 250 mm in width, with a thinned section measuring 37.5 mm in thickness. The arch specimens were constructed from two types of materials: CF50-grade steel fiber-reinforced concrete and C50-grade traditional reinforced concrete. The specimens are depicted in Figure 1 and Component diagram depicted in Figure 2.

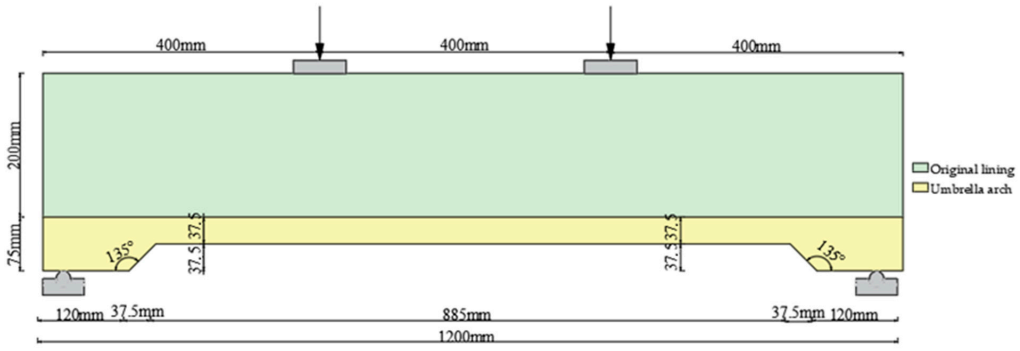

Figure 1. Composite sleeve arch.

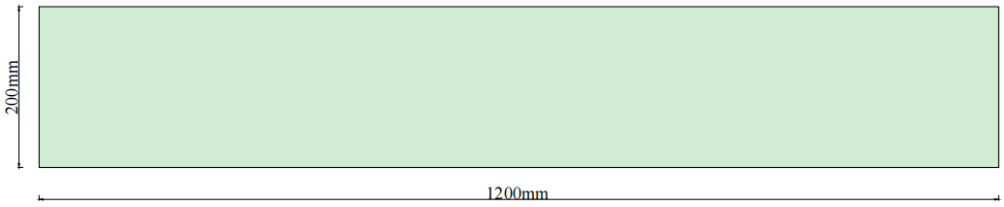

(**a**) Original lining

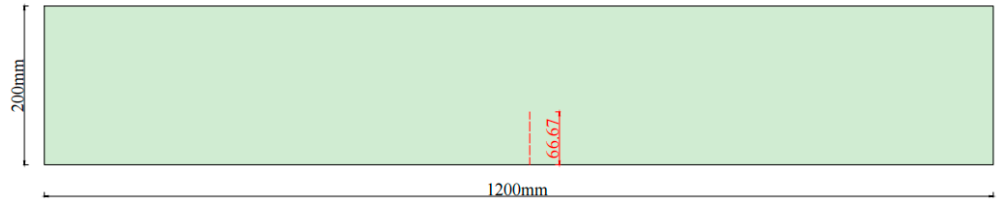

(**b**) 1/3 pre-cracked original lining

Figure 2. *Cont.*

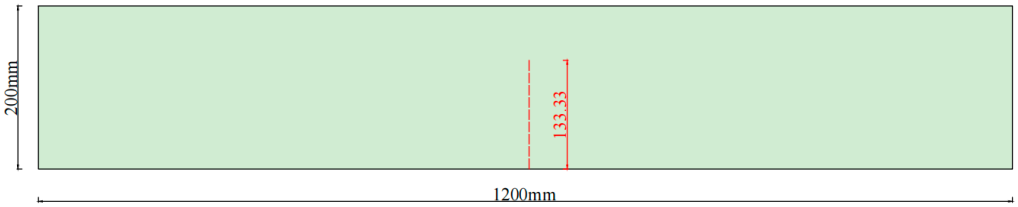

(**c**) 2/3 pre-cracked original lining

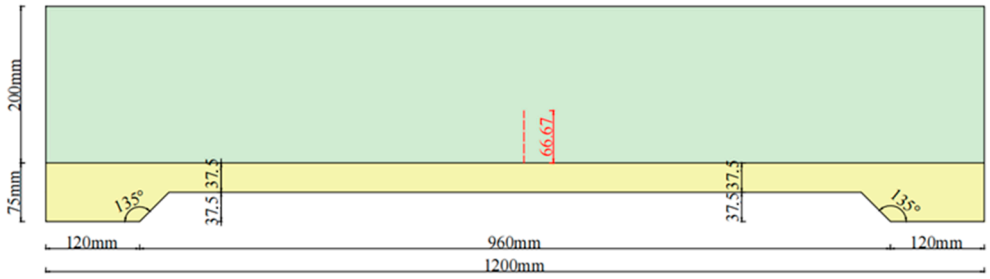

(**d**) composite arch reinforcement 1/3 prefabricated crack lining

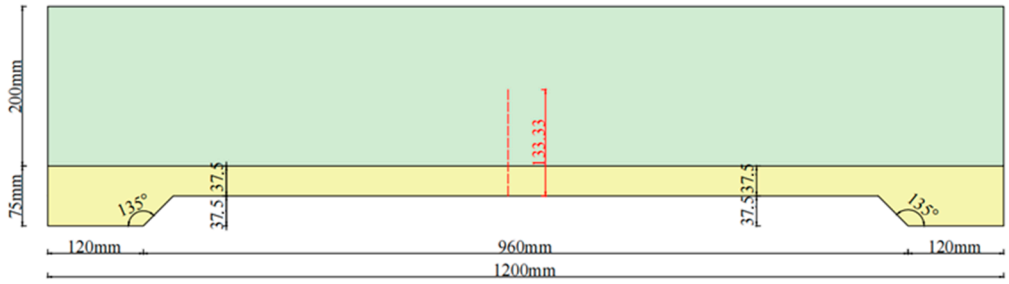

(**e**) composite arch reinforcement 2/3 prefabricated crack lining

Figure 2. Component diagram: (**a**) component 1; (**b**) component 2; (**c**) component 3; (**d**) component 4; (**e**) component 5.

In this study, loads were applied to the original, prefabricated crack, and composite linings using special loading devices, as depicted in Figure 3. Before testing, the surfaces of the specimens were polished and painted to enhance observational clarity during experiments. Strain gauges were installed on the front, and sides, adjacent to the prefabricated cracks at the center, and at the variable cross-section of the umbrella arch. Additionally, dial indicators were positioned at the mid-span and the lower extremities of the loading ends, and the data acquisition system was activated at the start of loading, while the pouring of the specimens is illustrated in Figure 4.

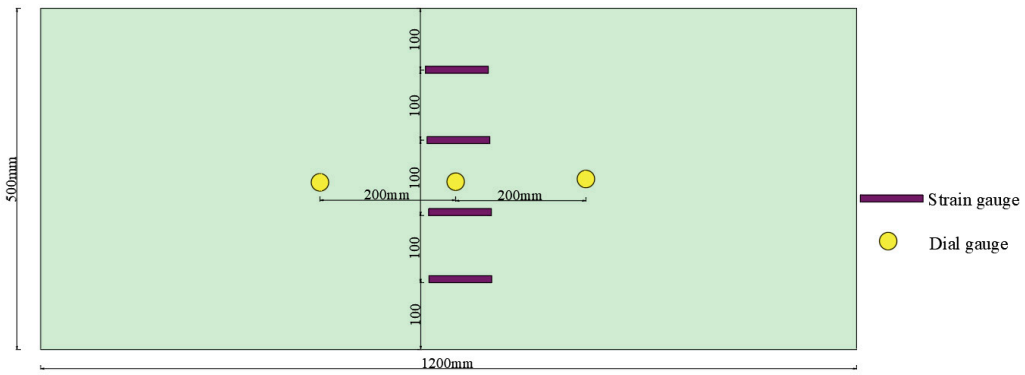

(**a**) Top view

Figure 3. *Cont.*

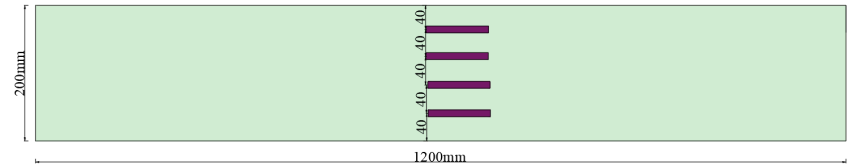

(**b**) Side view of the original lining

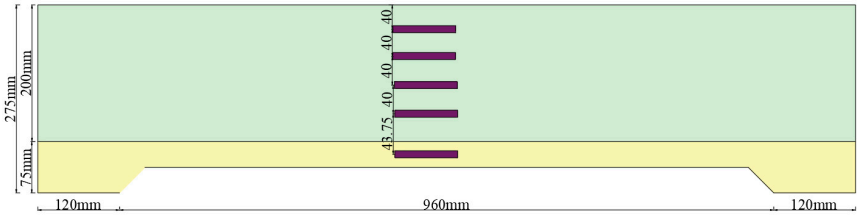

(**c**) Side view of the composite sleeve arch.

Figure 3. Schematic diagram of strain gauge and dial gauge positions.

Figure 4. Specimen loading.

2.3. Experimental Preparation and Loading

During the loading process, the test component was secured at both ends using fixed and movable hinge supports. A hydraulic jack was utilized to apply a vertical load to the test specimen, incrementally increasing by 10 KN until the specimen failed.

3. Experimentation Results

3.1. Reinforcement Performance of Steel Fiber-Reinforced Concrete

(1) Concrete strain at the variable cross-section

The strain was measured by installing strain gauges at the umbrella arch location under an external load of 1000 KN; the concrete in the 1/3 and 2/3 prefabricated crack components strengthened by the umbrella arch exhibited maximum compressive strains of −1021 με and −1431 με, respectively. Under this loading condition, the maximum compressive strain in the concrete at the variable cross-section met the design specifications and did not result in crushing.

(2) Surface concrete strain near prefabricated cracks

The strain was measured using strain gauges positioned near the prefabricated cracks. After collecting and analyzing the test data, the maximum compressive strains of concrete near the prefabricated cracks amounted to −605 με and −852 με for the 1/3 and 2/3 prefabricated crack components, respectively, reinforced by the umbrella arch under an external load of 500 KN. Under an external load of 1000 KN, the maximum compressive strains of the concrete near the prefabricated cracks were −1256 με and −1752 με for the 1/3 and 2/3 prefabricated crack components, respectively, reinforced by the umbrella arch. Under this load, the maximum compressive strain of the surface concrete near the prefabricated cracks met the design specifications and did not result in any crushing.

(3) Distortion

As shown in Figure 5a, components 1, 2, and 3 exhibit brittle failure under load, and the rate of change in mid-span distortion increases progressively with increasing load. Under the same load, mid-span distortion increases as the degree of cracking increases; components 4 and 5 exhibit relatively minor mid-span distortions before damage as the load increases. Component 1 fails under a load of 700 KN, components 2 and 3 fail at 550 KN, and components 4 and 5 do not fail even under a load of 1000 KN. The mid-span distortions for components 1, 2, 3, 4, and 5 under the respective loads measure 5.01 mm, 4.78 mm, 6.31 mm, 3.25 mm, and 3.57 mm, respectively.

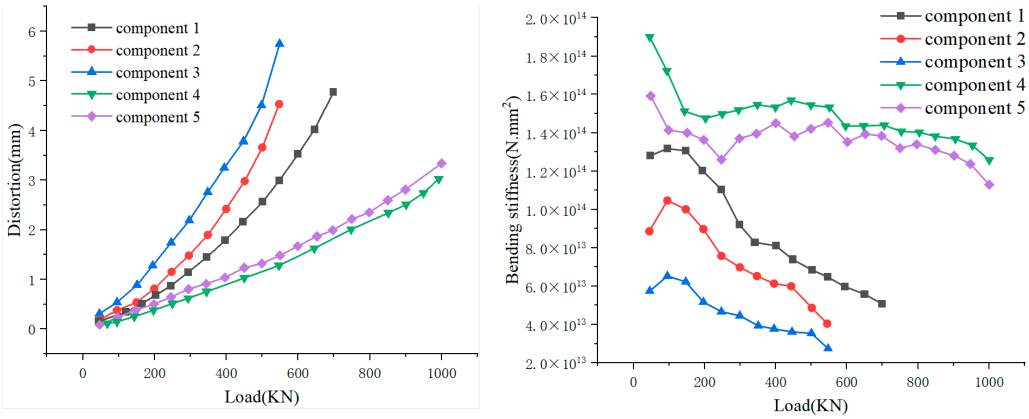

(**a**) Distortion (**b**) Bending stiffness

Figure 5. The variation of distortion and bending stiffness with load.

As depicted in Figure 5b, as the load increases, there is a general decrease in the bending stiffness of the components. For component 4, stiffness decreases sharply between 0 and 200 KN, and cracking occurs along the prefabricated lines. Stiffness remains relatively stable between 200 and 600 KN, during which the original lining and the umbrella arch are co-stressed, resulting in cracks within the umbrella arch. Between 600 and 1000 KN, the original lining nears destruction. Concurrently, the umbrella arch, now bearing the load independently, shows further stiffness reduction, more extensive cracking, and transition of the component into a plastic state. For component 5, stiffness decreases sharply between 0 and 150 KN, with cracking along the prefabricated lines. Between 150 and 500 KN, stiffness is relatively stable with a slight upward trend; the force on the original lining decreases while that on the umbrella arch increases, leading to further cracking. Between 500 and 1000 KN, the load-bearing capacity of the arch decreases significantly, prompting the components to transition to a plastic state and commence degradation. Under load, the stiffness of components 1, 2, and 3 decreases markedly, exhibiting brittle failure.

3.2. Reinforcement Performance of Reinforced Concrete

(1) Concrete strain at the variable cross-section

Strain measurements were obtained using strain gauges affixed to the umbrella arch after collecting and analyzing the test data. The maximum compressive strains recorded were −1021 με and −1431 με in the scenarios where 1/3 and 2/3 prefabricated crack components, respectively, were reinforced by the umbrella arch under an external load of 950 KN. This suggests that the concrete experienced crushing under the external load it was designed to withstand.

(2) Surface concrete strain near prefabricated cracks

The strain was measured by posting strain gauges near the prefabricated cracks, and by collecting and sorting out the test data, the maximum compressive strains of concrete near the prefabricated cracks were −715 με and −985 με when the 1/3 prefabricated crack components and 2/3 prefabricated crack components were strengthened by the umbrella

arch under the external load of 550 KN. When the external load is 950 KN, the maximum compressive strain of the concrete near the prefabricated crack was −1669 με and −2452 με, respectively, when the 1/3 prefabricated crack component and 2/3 prefabricated crack component are strengthened by the umbrella arch. Under the set load, the maximum compressive strain of the surface concrete near the prefabricated crack meets the design requirements and is not crushed. It can be concluded that the concrete is crushed under the external load of its design.

(3) Distortion

As depicted in Figure 6a, components 1, 2, and 3 exhibit brittle failure under load, with the rate of mid-span distortion increasing gradually as the load increases; additionally, under consistent load conditions, mid-span distortion escalates with increasing crack severity. Components 4 and 5 demonstrate relatively minor mid-span distortions prior to failure as the load increases. When the load reaches 900 KN, the rate of increase in mid-span distortion accelerates sharply, resulting in the failure of the component. Under the same load conditions, mid-span distortion of the reinforced members intensifies as crack severity increases. The mid-span distortions of components 1, 2, 3, 4, and 5 under the respective loads measure 5.01 mm, 4.78 mm, 6.31 mm, 5.16 mm, and 5.48 mm, respectively.

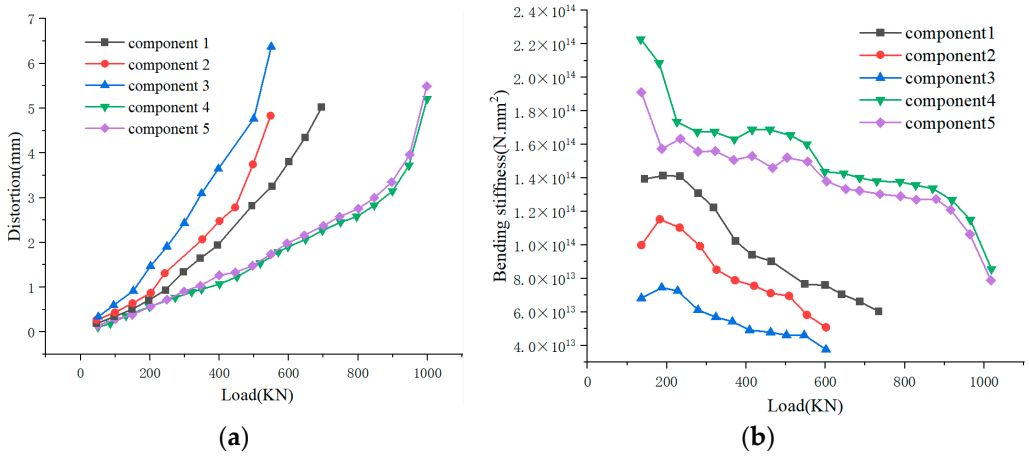

(**a**) (**b**)

Figure 6. The variation of deflection and bending stiffness with load: (**a**) distortion; (**b**) bending stiffness.

As depicted in Figure 6b, as the load increases, the bending stiffness of the components generally decreases. For component 4, stiffness decreases sharply from 0 to 1500 KN, and cracking occurs along the prefabricated lines. Stiffness remains relatively stable between 1500 and 450 KN, during which the original lining and the umbrella arch are co-stressed, resulting in cracks forming within the umbrella arch. Between 450 and 900 KN, the original lining nears destruction. Concurrently, the arch, now bearing the load independently, shows a gradual decrease in stiffness and further cracking. Beyond 900 KN, component stiffness decreases sharply, leading to component failure. For component 5, stiffness decreases sharply between 0 and 100 KN, with cracking occurring along the prefabricated lines. Between 100 and 400 KN, stiffness remains relatively stable; however, as the original lining and the umbrella arch are co-stressed, the arch bears a greater load, leading to additional cracking. Between 400 and 850 KN, extensive cracking in the arch leads to a sharp decrease in its load-bearing capacity, culminating in component failure. Stiffness in components 1, 2, and 3 decreases sharply under load, exhibiting brittle failure.

4. Establishment of Numerical Test Model

4.1. Model Profile

To simulate the stress of the composite arch more realistically, the arch, the original lining, and the waterproof plate in the model are simulated by entity units. Using hexahedral meshes to divide entity units can effectively improve computing quality. This

study mainly analyzes the force condition at the prefabricated cracks, so the grid at the prefabricated cracks is encrypted. Figure 7a shows the original lining numerical model, Figure 7b shows the 1/3 prefabricated crack lining, and Figure 7c shows the prefabricated crack lining reinforced by the arch, and 2/3 prefabricated crack lining reinforced arch.

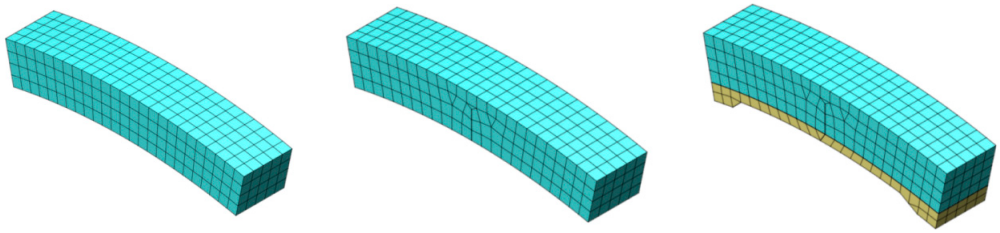

(**a**) (**b**) (**c**)

Figure 7. Numerical model. (**a**) Original lining. (**b**) Prefabricated crack original lining. (**c**) Arch reinforcement of prefabricated crack lining.

4.2. Material Parameter

The calculation parameters for concrete, steel bars, and steel fiber concrete are determined based on the concrete structure design codes, the steel fiber concrete design standards, and other relevant information, As shown in Table 1.

Table 1. Main physical and mechanical parameters of materials.

Material	Density (KN/m^3)	Elastic Modulus (Mpa)	Poisson Ratio
C50 steel fiber-reinforced concrete	25.0	34,500	0.20
Steel reinforcement	78.5	200,000	0.30
C25 concrete	25.0	28,000	0.20
Waterproof plate	8.6	10	0.45

4.3. Material Constitutive Model

4.3.1. Concrete Constitutive Model

The total strain crack model in MIDAS/FEA can better reflect the mechanical properties of concrete materials and steel fiber concrete materials. The Thorenfeldt compression model is used for the compression model, and the brittle model is used for the tensile model.

(1) Compressive Constitutive Model

As shown in Figure 8, the Thorenfeldt compression curve illustrates the behavior of concrete under compressive load. The Thorenfeldt compression model in MIDAS/FEA effectively accounts for the compressive properties of concrete [24,25].

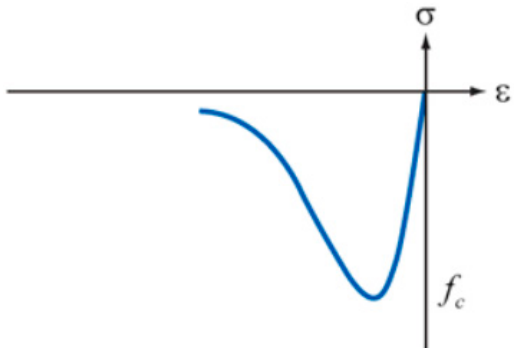

Figure 8. Thorenfeldt compression curve.

(2) Tensile Constitutive Model

Due to the inherent properties of concrete, its tensile strength is relatively low. In this study, the "Brittle model" from the tensile model in MIDAS/FEA is chosen as the constitutive model for concrete under tension. As shown in Figure 9, when the tensile stress in the material exceeds its design tensile strength, the tensile stress does not increase further and drops to zero.

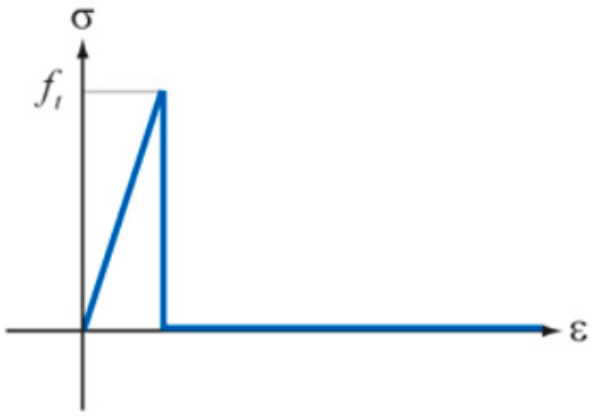

Figure 9. Brittle model.

4.3.2. Steel Constitutive Model

The von Mises model in MIDAS/FEA was used for the steel bar in this study. The von Mises criterion comprehensively considers the stresses in different directions for anisotropic materials and can be used to represent material strength under complex stress states. Moreover, the von Mises model assumes that the yield behavior of materials follows a linear elastic–plastic model, which is typically applicable to metallic materials. Based on numerous references [26–29], the strain corresponding to the ultimate stress for the reinforcing steel in this study is taken as 0.025, as shown in Figure 10.

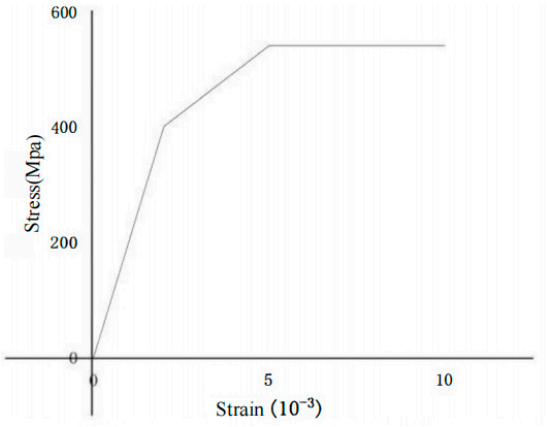

Figure 10. Stress–strain curve of steel bar.

4.3.3. Contact Surface Configuration

This study primarily focuses on the contact surfaces between the linings, sleeve arches, and waterproof boards. According to the relevant literature, the friction coefficient between rubber and concrete ranges from 0.6 to 0.9. Based on relevant studies, the stiffness adjustment coefficient is set to 1, and the friction coefficient is set to 0.6.

4.4. Simulated Calculation Conditions

At both ends of the model, the displacements in the X, Y, and Z directions are constrained, and vertical loads are applied to both sides of the prefabricated cracks. In this section, the strain in the concrete near the prefabricated cracks, the strain on the thinned surfaces, and the displacement deflections of the pipes under various loads are analyzed sequentially. Loading process: The vertical load increases by 50 KN per stage, and upon reaching 1000 KN, the application of the load concludes.

5. Modeling Results

5.1. Reinforcement Performance of Different Materials at Variable Cross-Section

This study primarily investigates the reinforcing effects of two distinct materials—steel fiber concrete and reinforced concrete—on varying degrees of lining crack damage at the variable sections of the arch. The stress concentration areas of these materials at the variable cross-sections are numerically analyzed, and the stress values at five characteristic points (A, B, C, D, and E) are determined; each characteristic point is depicted in Figure 11. Due to space constraints, only the load–stress curves for component 4, reinforced with two different materials, are presented.

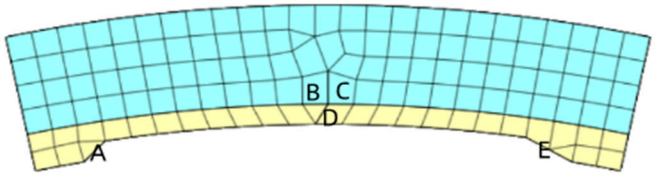

Figure 11. Numerical model.

Under varying load conditions, the load–stress correlation curves at Points A and E are illustrated in Figure 12. The diagrams reveal that at Points A and E, the load and stress for both materials—reinforced concrete and steel fiber concrete—are approximately proportional. Under identical loading conditions, the stress in steel fiber concrete exceeds that in reinforced concrete, though the difference is marginal.

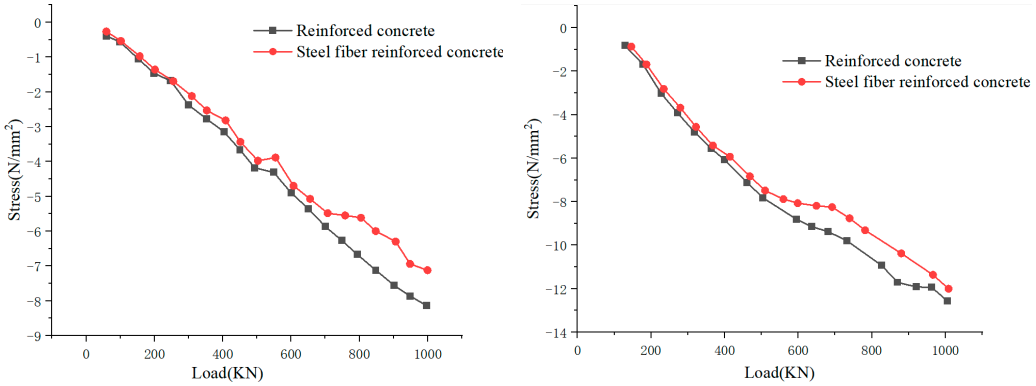

(**a**) Point A (**b**) Point E

Figure 12. Relationship curve between load and stress.

Under varying load conditions, the load–stress correlation curves at Points B and C are illustrated in Figure 13. The figure illustrates that, in the initial loading stages, the concrete on both sides of the crack predominantly undergoes compression. Upon reaching a specific load threshold, the compressive stress diminishes, and the arch, along with the original lining, begins to share the load. However, as the load increases, the concrete transitions to a tensile state, with tensile stress escalating primarily in the arch. Furthermore, the stress in the reinforced concrete exceeds that in the steel fiber-reinforced concrete.

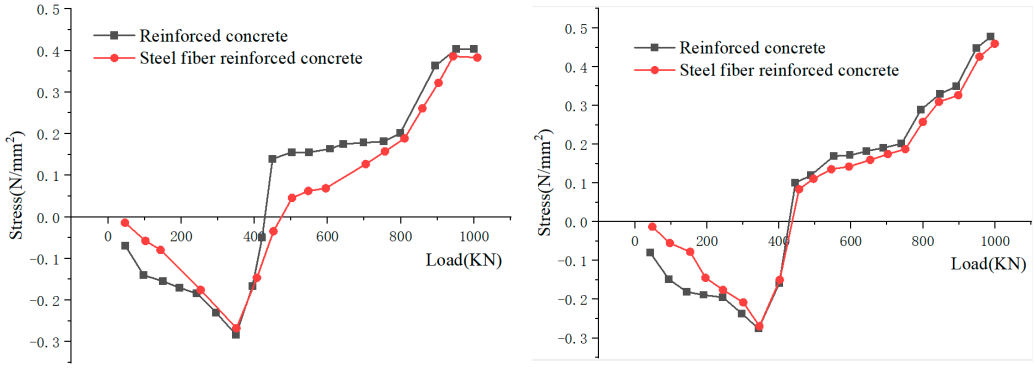

(**a**) Point B (**b**) Point C

Figure 13. Relationship curve between load and stress.

Under varying load conditions, the load–stress correlation curve at Point D is depicted. As depicted in Figure 14, during the initial loading stages, the concrete at the composite surface of the arch and lining primarily undergoes compression. Upon reaching a specific load, the compressive stress diminishes. Concurrently, the arch and the original lining share the load, resulting in cracks at the composite surface. As the load increases, cracks at the composite surface continue to widen, and the concrete predominantly experiences tension. Under identical design loads, the stress in reinforced concrete at concentrated stress regions (A, B, C, D, and E) exceeds that in steel fiber-reinforced concrete by 16.15%, 6.01%, 12.68%, 36.62%, and 4.82%, respectively, the reinforcement performance of steel fiber-reinforced concrete is superior to that of reinforced concrete. Additionally, this difference is more pronounced in the mid-span region.

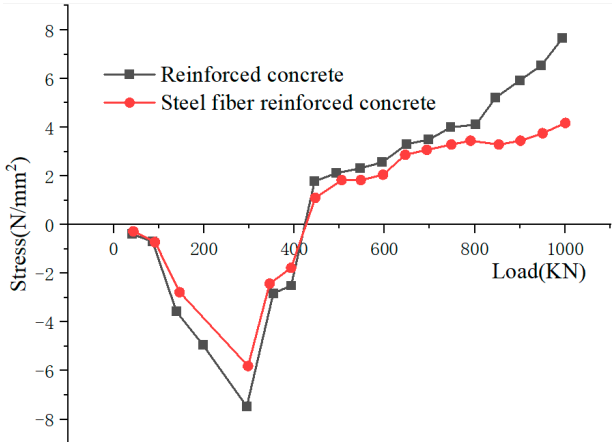

Figure 14. Relationship curve between load and stress at Point D.

The reinforcement effects of two materials on various damaged linings were compared and analyzed. During the initial loading stages, the overall stiffness of the reinforced concrete damaged lining exceeds that of the steel fiber-reinforced concrete; however, as the load increases, the overall stiffness of the steel fiber-reinforced concrete damaged lining surpasses that of the reinforced concrete. The steel fiber-reinforced concrete damaged lining undergoes plastic failure under the design conditions without component destruction, whereas the reinforced concrete damaged lining incurs damage under the same conditions. In the stress concentration areas (A, B, C, D, and E), the stress in the steel fiber-reinforced concrete damaged lining is less than that in the reinforced concrete. Based on the analysis, the reinforcement performance of steel fiber-reinforced concrete is superior to that of reinforced concrete, with both materials meeting the structural stress requirements.

5.2. Influence of Variable Section Thickness of Sleeve Arch on Reinforcement Performance

According to the experimental results, the material used at the variable section of the arch is steel fiber concrete. To further explore the impact of the thickness of the variable section on the reinforcement effectiveness of the steel fiber arch while adhering to building constraints, the thickness varied (50 mm, 60 mm, 75 mm, 85 mm, and 100 mm) with all other parameters held constant.

5.2.1. Reinforcement Performance of the Medium Crack Lining

As shown in Figure 15, the stress at Point A in a thin sleeve arch of varying thicknesses is directly proportional to the load and inversely proportional to the thickness. In the initial loading stages, the stress at Point A in thin arches of different thicknesses is approximately uniform; however, as the load increases, the stress also gradually increases. Thin sleeve arches with thicknesses of 50 mm, 60 mm, 75 mm, 85 mm, and 100 mm exhibit compressive stresses at Point A of -7.942 N/mm^2, -7.815 N/mm^2, -6.707 N/mm^2, -6.403 N/mm^2, and -4.903 N/mm^2, respectively, when subjected to a load of 1000 KN.

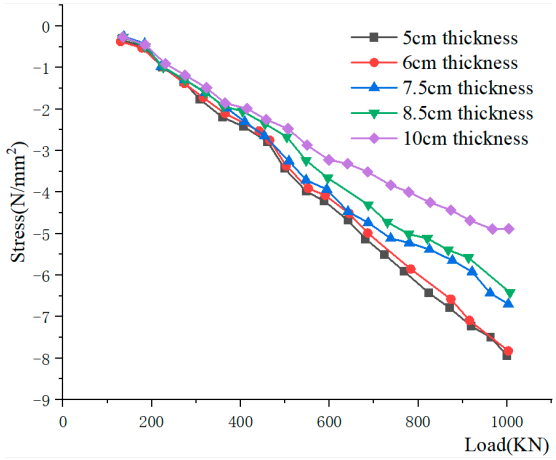

Figure 15. Relationship curve between load and stress at Point A.

As depicted in Figure 16a, during the initial stages of loading, the thin arch at Point B is predominantly subjected to compression. Upon reaching a specific load, the compressive stress diminishes, and the arch, along with the original lining, begins to share the load. As the load increases, the concrete at Point B primarily experiences tension, and the tensile stress gradually escalates. At a load of 1000 KN, the thin arches at Point B with thicknesses of 50 mm, 60 mm, 75 mm, 85 mm, and 100 mm exhibited tensile stresses of 0.503 N/mm^2, 0.445 N/mm^2, 0.382 N/mm^2, 0.369 N/mm^2, and 0.293 N/mm^2, respectively.

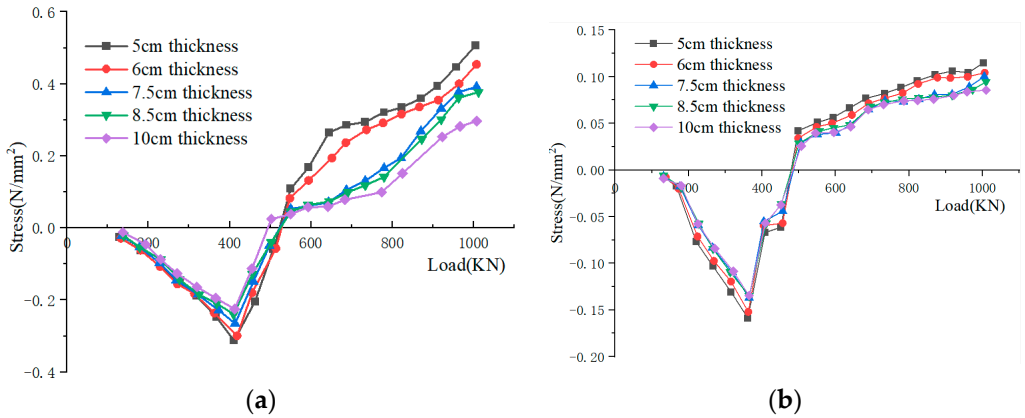

Figure 16. Relationship curve between load and stress: (**a**) Point B; (**b**) Point D.

As depicted in Figure 16b, during the initial stages of loading, the concrete in thin arches of varying thicknesses is primarily compressed at the composite surface at Point D of the arch and lining. Upon reaching a specified load, the compressive stress diminishes. As the load increases, the concrete at the composite surface primarily experiences tension. At a load of 1000 KN, thin arches at Point D with thicknesses of 50 mm, 60 mm, 75 mm, 85 mm, and 100 mm exhibited tensile stresses of 0.094 N/mm^2, 0.087 N/mm^2, 0.080 N/mm^2, 0.077 N/mm^2, and 0.072 N/mm^2, respectively.

5.2.2. Reinforcement Performance of the Severely Cracked Lining

As shown in Figure 17, the stress in thin sleeve arches of varying thicknesses at Point A is directly proportional to the load and inversely proportional to the thickness. Despite initial similarities, as the load increases, the stress gradually escalates. Thin sleeve arches at Point A, with thicknesses of 50 mm, 60 mm, 75 mm, 85 mm, and 100 mm, exhibit compressive stresses of −10.713 N/mm^2, −10.450 N/mm^2, −7.832 N/mm^2, −7.625 N/mm^2, and −7.356 N/mm^2, respectively, under a load of 1000 KN.

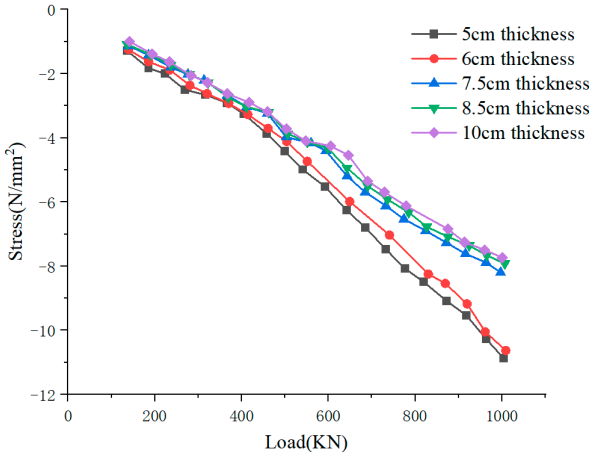

Figure 17. Relationship curve between load and stress at Point A.

As depicted in Figure 18a, during the initial stages of loading, the thin arch at Point B is primarily subjected to compression. Upon reaching a specific load, the compressive stress decreases, and the arch, along with the original lining, begins to share the load. As the load increases, the concrete at Point B predominantly experiences tension, and the tensile stress gradually escalates. At a load of 1000 KN, the thin arches at Point B with thicknesses of 50 mm, 60 mm, 75 mm, 85 mm, and 100 mm exhibited tensile stresses of 0.753 N/mm^2, 0.715 N/mm^2, 0.653 N/mm^2, 0.611 N/mm^2, and 0.471 N/mm^2, respectively.

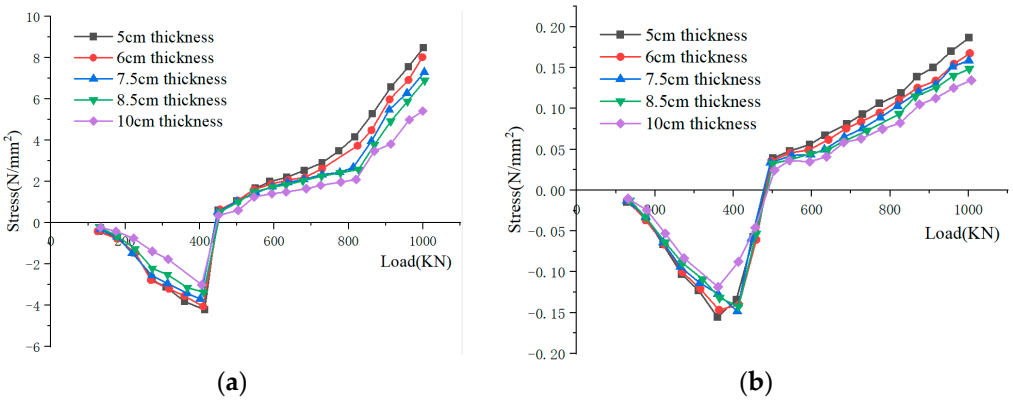

Figure 18. Relationship curve between load and stress: (**a**) Point B; (**b**) Point D.

As depicted in Figure 18b, during the initial stages of loading, the concrete at the composite surface of the sleeve arch and lining is predominantly compressed. Upon reaching a specified load, the compressive stress diminishes. As the load increases, the concrete at the composite surface primarily experiences tension. At a load of 1000 KN, the thin arches at Point D with thicknesses of 50 mm, 60 mm, 75 mm, 85 mm, and 100 mm exhibited tensile stresses of 0.187 N/mm^2, 0.171 N/mm^2, 0.158 N/mm^2, 0.150 N/mm^2, and 0.138 N/mm^2, respectively.

6. Conclusions

In this study, the reinforcement effects of thin sleeve arches with various materials and thicknesses on differently damaged linings are investigated through numerical simulations and model testing. After organizing and analyzing the test data and simulation results, the following conclusions are drawn:

(1) Comparative analysis of two kinds of materials for different damage lining reinforcement effects; both steel fiber-reinforced concrete and reinforced concrete can meet the requirements of structural stress. In the early stages of loading, the overall stiffness of damaged linings reinforced with reinforced concrete is greater than that of those reinforced with steel fiber-reinforced concrete. However, as the load increases, the overall stiffness of damaged linings reinforced with steel fiber-reinforced concrete becomes greater than that of those reinforced with reinforced concrete. Additionally, damaged linings reinforced with steel fiber-reinforced concrete exhibit plastic deformation under the design load without experiencing failure; however, damaged linings reinforced with reinforced concrete fail under the design load. In summary, the reinforcement performance of steel fiber-reinforced concrete is superior to that of traditional reinforced concrete.

(2) Under the design load, the thin arches of different thicknesses are loaded on the medium-cracked lining, which can meet the force requirements. Through comparative analysis, under the same load, the 10 cm thin arch has the best reinforcement performance, followed by 7.5 cm and 8.5 cm, and the 5 cm and 6 cm thin arches have the worst reinforcement performance. If only economic benefits are considered, 6 cm thin arches can be used in the reinforcement of medium-cracked linings, but considering its long-term reinforcement performance and economy, 7.5 cm is optimal.

In China, a significant number of operational tunnels have developed varying degrees of cracking and water leakage over time, seriously threatening structural integrity and traffic safety. In the field of tunnel lining reinforcement, the use of cast-in-place concrete arches is common; however, the long construction period presents challenges in ensuring construction quality. Experimental research on using prefabricated steel fiber-reinforced concrete arches for reinforcing cracked linings in confined spaces indicates that steel fiber-reinforced concrete has significant potential for the rapid and practical repair of deteriorated tunnels, and these findings underscore the importance of promoting this technology in the field.

Author Contributions: Y.Z.: conceptualization, supervision, validation, funding acquisition. Z.L.: conceptualization, methodology, investigation, and data curation. L.L.: writing—original draft, writing—review and editing. J.Z.: visualization, resources, and supervision. All authors have read and agreed to the published version of the manuscript.

Funding: This research was funded by the Guangdong Province Key Areas R & D Program (2022B0101070001), and the National Natural Science Foundation of China (No. 52078089, No. 52274176, No. 52078090), and the Chongqing Natural Science Foundation (cstc2021jcyj-msxmX1075), and the Chongqing Natural Science Foundation Innovation and Development Joint Fund (2022NSCQ-LZX0285), and the Chongqing Municipal Education Commission "Shuangcheng Economic Circle Construction in Chengdu-Chongqing Area" Science and Technology Innovation Project (KJCX2020031).

Institutional Review Board Statement: Not applicable.

Informed Consent Statement: Not applicable.

Data Availability Statement: The data will be made available upon request. The corresponding author should be contacted if someone wants to request the data from this study.

Conflicts of Interest: Author Yu Zhou was employed by the company Guangdong Hualu Transport Technology Co., Ltd. The remaining authors declare that the research was conducted in the absence of any commercial or financial relationships that could be construed as a potential conflict of interest.

References

1. He, C.; Wang, B. Research progress and development trends of highway tunnels in China. *J. Mod. Transp.* **2013**, *21*, 209–223. [CrossRef]
2. Wang, X.; Lai, J.; Qiu, J.; Xu, W.; Wang, L.; Luo, Y. Geohazards, reflection and challenges in Mountain tunnel construction of China: A data collection from 2002 to 2018. *Geomat. Nat. Hazards Risk* **2020**, *11*, 766–785. [CrossRef]
3. Yang, C.; Hu, Q. Research on disease detection and treatment technology of highway tunnel, China. *Mod. Tunn. Technol.* **2021**, *58*, 237–245.
4. Zhang, N.; Zhu, X.; Ren, Y. Analysis and Study on Crack Characteristics of Highway Tunnel Lining. *Civ. Eng. J.* **2019**, *15*, 1119–1123. [CrossRef]
5. Wang, P.; Wan, F.; Hao, X. Study on optimization of lining structure reinforcement scheme of Dugongling tunnel. *J. Highw. Transp. Res. Dev.* **2021**, *30*, 32–38.
6. Xu, C.; Wang, H. Engineering geological characteristics and engineering hazard analysis of Dugongling Tunnel. *J. Highw. Transp. Res. Dev.* **2019**, *36*, 93–99.
7. Meng, J. Cause analysis and prevention measures of highway tunnel lining cracks, China. *Transp. World* **2023**, *Z1*, 282–285.
8. Tang, C.; Liu, C.; Feng, X. Analysis of crack propagation mechanism of existing tunnel lining. *Sichuan Archit.* **2022**, *42*, 112–114.
9. An, D.; Chen, Z.; Meng, L.; Cui, G. Application of fiber-reinforced concrete lining for fault-crossing tunnels in meizoseismal area to improving seismic performance. *Adv. Mech. Eng.* **2020**, *12*, 1687814020944023. [CrossRef]
10. Hou, Q. Analysis of the application of steel fiber concrete technology in road and bridge construction. *Sichuan Build. Mater.* **2023**, *49*, 7–8+11.
11. Gong, X. Application of steel fiber reinforced concrete technology in road and bridge construction. *Creat. Living* **2021**, *10*, 56–57.
12. Congro, M.; de Alencar Monteiro, V.M.; de Andrade Silva, F.; Roehl, D.; Brandão, A.L.T. A novel hybrid model to design fiber-reinforced shotcrete for tunnel linings. *Tunn. Undergr. Space Technol.* **2023**, *132*, 104881. [CrossRef]
13. Liu, S. The Application of Steel Fiber Concrete Technology in Highway Bridge Construction. *Constr. Mach. Maint.* **2022**, *2*, 84–85.
14. Tian, Z.; Liu, B. Application Research on Superimposed Arch Reinforcement Technology of Highway Tunnel. *Highway* **2021**, *66*, 339–344.
15. Yang, Y. Discussion on the application of composite arch reinforcement technology in highway tunnel. *TranspoWorld* **2022**, *30*, 52–54.
16. Su, C.; An, N.N.; Wang, Z. Mechanical properties of shotcrete arch reinforcement structure of highway tunnel. *J. Archit. Civ. Eng.* **2020**, *37*, 203–213.
17. Wang, X.; Fan, F.; Lai, J.; Xie, Y. Steel fiber reinforced concrete: A review of its material properties and usage in tunnel lining. *Structures* **2021**, *34*, 1080–1098. [CrossRef]
18. Hu, X. Application and Research of Steel Fiber Reinforced Concrete in Tunnel Construction. Ph.D. Thesis, Shijiazhuang Railway University, Shijiazhuang, China, 2023.
19. Cui, G.; Sun, L.; Zuo, K.; Wang, M.; Jing, H. Review on mechanical properties of fiber-reinforced concrete tunnel lining. *Mod. Tunn. Technol.* **2019**, *56*, 1–7.
20. He, X. Application of steel fiber in tunnel shotcrete. *Resour. Inf. Eng.* **2022**, *37*, 90–92+96.
21. Wu, L.; Yan, Z. Application analysis of steel fiber reinforced concrete technology in road and bridge construction. *Sci. Technol. Innov.* **2024**, *7*, 173–175.
22. Huang, J. Experimental Study on Mechanical Properties and Impermeability of Hybrid Fiber Reinforced Concrete. Ph.D. Thesis, Wuhan Institute of Technology, Wuhan, China, 2012.
23. Cao, Y. Experimental study on the influence of steel fiber type on the properties of steel fiber reinforced concrete. *J. Lanzhou Jiaotong Univ.* **2019**, *38*, 1–8.
24. Thorenfeldt, E. Mechanical properties of high- strength concrete and applications in design. In Proceedings of the Symptom Utilization of High-Strength Concrete, Stavanger, Norway, 15–18 June 1987.
25. Zhou, N.; Wang, L.; Wang, G.; Yang, N. Analysis of seismic performance of semi-rigid connection steel frame. *Ind. Build.* **2009**, *39*, 112–115+85.
26. Luo, Q. Nonlinear finite element analysis of connections between concrete-filled square steel tubular columns and steel beams. *J. China Three Gorges Univ. (Nat. Sci. Ed.)* **2010**, *32*, 45–47.
27. Wang, Y.; Wang, S.; Wang, Z.; Du, D.; He, J. Stress analysis of complex joints with over-limit elevation based on ABAQUS substructure method. *Archit. Sci.* **2012**, *41*, 655–661.

28. Pan, J.; Wang, Z.; Zhang, J. Nonlinear finite element analysis of frame composite beam-column joints. *J. Xi'an Univ. Archit. Technol. (Nat. Sci. Ed.)* **2009**, *41*, 655–662.
29. Teng, Z.; Zhu, J. *Concrete Structure and Masonry Structure*; China Architecture and Technology Press: Beijing, China, 2013; Volume 9.